RSC
Applied Interfaces

ROYAL SOCIETY
OF CHEMISTRY

PAPER

View Article Online
View Journal | View Issue

Check for updates

Cite this: *RSC Appl. Interfaces*, 2026, **3**, 95

Chemoresistive properties of NiO surface-modified Nb-doped TiO_2 mesoporous thin films

Muhammad Hamid Raza, †*[a] Simona Crispi,†[b] Estelle Jozwiak,[c] Marvin Frisch,[d]
Ralph Kraehnert,[d] Rutger Schlatmann, [a] Daniel Amkreutz,[a]
Giovanni Neri [b] and Nicola Pinna [c]

Received 19th September 2025,
Accepted 4th November 2025

DOI: 10.1039/d5lf00279f

rsc.li/RSCApplInter

Functionalized metal oxide thin films are widely applicable in heterogeneous catalysis and gas sensing due to their distinct electrochemical properties. Given their importance in practical applications, developing a comprehensive understanding of their chemoresistive behavior is essential, which requires the precise engineering of thin-film-based nanostructures. Here, we report the on-chip fabrication of mesoporous Nb-doped titania ($Nb_xTi_{1-x}O_2$) thin films with template-controlled mesoporosity *via* dip-coating and subsequent calcination on conductometric transducers. The pore wall surfaces of mesoporous $Nb_xTi_{1-x}O_2$ films were surface-modified with variable NiO loadings *via* atomic layer deposition (ALD) to produce NiO-loaded $Nb_xTi_{1-x}O_2$ thin films (XNiO–$Nb_xTi_{1-x}O_2$). The NiO loading was controlled by adjusting the number of ALD cycles (X = 5–200). The chemoresistive properties of the synthesized mesoporous $Nb_{-}Ti_{1-x}O_2$ and XNiO–$Nb_xTi_{1-x}O_2$ thin films were investigated under different environmental conditions, namely oxidizing and reducing gases. The XNiO–$Nb_xTi_{1-x}O_2$ thin films showed an enhanced response to reducing gases, particularly acetone and ethanol, compared to unloaded mesoporous $Nb_xTi_{1-x}O_2$. Among them, 5NiO–$Nb_xTi_{1-x}O_2$, featuring discontinuous NiO-decorated species, exhibits the strongest response to acetone. The superior sensing performance of the on-chip fabricated 5NiO–$Nb_xTi_{1-x}O_2$ sensor toward acetone is attributed to the high surface area of the mesoporous thin films and surface-modification with NiO species, which enhances the sensing properties through chemical sensitization.

1. Introduction

Semiconducting metal oxides (SMOXs) have garnered considerable attention for sustainable technological applications due to their favorable intrinsic properties such as wide availability, low cost, environmental compatibility, non-toxicity, robust chemical stability, and relatively small band gaps.[1] Their excellent performance across various fields and economic feasibility have positioned them among the most widely researched functional materials. The electronic and electrochemical characteristics of transition metal oxides have been extensively explored over the past decades, driven by their versatility in applications such as catalysis, photovoltaics, optoelectronics, and chemical sensing.[1–4] Specifically, the chemoresistive behavior of nanostructured SMOXs has proven essential for the development of next-generation, high-performance gas sensors.[5] The chemoresistive properties of SMOX heterostructures are often ascribed to a complex interplay of electronic, chemical, and structural effects.[2,6] A comprehensive understanding of the chemoresistive properties at heterointerfaces remains elusive, particularly for predictive modeling.[7] One critical challenge lies in the structural ambiguity of many heterostructures, where both constituent materials may be exposed to the environment, or the core is only partially enclosed by a non-homogeneous or ill-defined shell layer.[7] Gases may preferentially interact with one phase, while secondary reaction products affect the other, hence complicating the interpretation of the chemoresistive properties in the presence of analytes.[2,6,7] Therefore, constructing structurally controlled heterostructures at the nanoscale is imperative for unraveling material reactivity.[4]

The chemoresistive behaviors of heterostructured systems vary significantly and are not always associated with a single factor, such as heterojunctions.[2,6,7] In some cases, the response may arise predominantly from the core or the shell material. For instance, our previous investigations on NiO-coated carbon

---

[a] *PVcomB, Helmholtz-Zentrum Berlin für Materialien und Energie (HZB), Schwarzschildstrasse 3, 12489 Berlin, Germany.*
E-mail: hamid.raza@helmholtz-berlin.de
[b] *Department of Engineering, University of Messina, C.da Di Dio, I-98166 Messina, Italy*
[c] *Department of Chemistry and The Center for the Science of Materials Berlin, Humboldt-Universität zu Berlin, Brook-Taylor-Str. 2, 12489 Berlin, Germany*
[d] *Department of Chemistry, Technische Universität Berlin, Strasse des 17. Juni 124, 10623 Berlin, Germany*

† Authors contributed equally to this work.

nanotubes (CNTs) demonstrated that the gas response stemmed from the NiO shell only.[8] Conversely, in our other study, where a secondary metal oxide layer was conformally deposited onto pre-contacted one-dimensional SnO_2 nanowires, the observed gas responses were solely attributed to the core material.[9] Although the deposition altered the interfacial depletion region, the shell did not significantly affect the fundamental transduction behavior but only modified the surface characteristics of the prefabricated sensor and hence interaction with analytes.[9,10] Moreover, altering the fabrication sequence or architecture, such as incorporating shell–shell junctions in core–shell systems while avoiding direct core–core contact, can lead to transduction governed by the shell, the core, or the interface, depending on the device configuration.[2,6,7] Additionally, if the core material already exhibits sufficient electrical conductivity, a large surface-to-volume ratio, and intrinsic chemoresistive sensitivity, the sensing performance may be further amplified through chemical sensitization, catalytic or spillover effects.[2,11–13]

We leverage this approach by utilizing mesoporous TiO_2-based films as the primary high-surface-area substrate, serving as a model mesoporous SMOX. Titania was selected due to its tunable electrical conductivity (*e.g.*, *via* transition metal doping) and chemical stability, while offering nanostructured porosity which is known to enhance solid–gas interactions, facilitate gas diffusion and promote mass-transfer kinetics.[14–16] The addition of niobium at a concentration of 35 mol % has been found to increase the electrical conductivity while preserving the mesoporous TiO_2-based framework (*via* dip-coating and subsequent calcination), thereby facilitating efficient gas diffusion and charge transport.[14] The Nb-doped mesoporous TiO_2 ($Nb_xTi_{1-x}O_2$) thin films directly fabricated on-chip *via* dip-coating and evaporation-induced self-assembly (EISA) were then surface-modified with controlled loadings of NiO species *via* atomic layer deposition (ALD). ALD was selected as a state-of-the-art technique for the deposition of homogeneous and conformal thin films over high-aspect ratio substrates, since it allows precise control over film thickness due to its self-limiting nature while preserving the intrinsic properties of the underlying substrate.[9,10]

The synthesized NiO-functionalized thin films are hereinafter denoted as XNiO–$Nb_xTi_{1-x}O_2$ (where X indicates the number of ALD cycles, ranging from 5–200). The chemoresistive behavior of the mesoporous $Nb_xTi_{1-x}O_2$ and XNiO–$Nb_xTi_{1-x}O_2$ films were evaluated using conductometric transducers, revealing an enhanced sensing response. This improvement is attributed to chemical sensitization effects, offering insight into the correlation between structure and sensing performance in engineered thin film systems.

2. Experimental section

2.1. Synthesis of NiO-loaded mesoporous Nb-doped TiO_2

Soft templated mesoporous titania and Nb-doped titania films were synthesized directly on conductometric platforms used as gas sensors. The transducers, consisting of interdigitated electrodes, were dip-coated using $TiCl_4$ and $NbCl_5$ precursors dissolved in ethanol, as described elsewhere.[14] A content of 35 mol % of Nb was previously found to yield the highest electrical sheet conductivity as we reported elsewhere.[14] NiO films were subsequently deposited onto the mesoporous Nb-doped TiO_2 framework *via* atomic layer deposition (ALD). The ALD process was performed using nickelocene [$Ni(Cp)_2$] and ozone (O_3, 20 wt% in O_2) in a thermal ALD system (GEMStar, Arradiance). The temperature of the reaction chamber and precursor manifolds was maintained at 200 °C and 115 °C, respectively. $Ni(Cp)_2$ (held at 90 °C in a stainless-steel bubbler) and ozone (at RT) were sequentially introduced into the chamber using Ar as both the carrier and purging gas. A typical ALD cycle consisted of: (i) a 2 s pulse of $Ni(Cp)_2$, (ii) a 40 s exposure of $Ni(Cp)_2$, (iii) a 30 s purge to remove the residual precursor, (iv) a 0.5 s pulse of O_3, (v) a 30 s exposure of O_3, and (vi) a 30 s purge to remove the excess of the reactant or by-products, if any. The NiO loading was controlled by varying the number of ALD cycles, ranging from 5 to 200. The resulting samples were denoted as (X)NiO–$Nb_xTi_{1-x}O_2$, where X indicates the number of ALD cycles. Further details of the NiO ALD process are reported elsewhere.[8,9,17]

2.2. Characterization

TEM imaging and selected-area electron diffraction (SAED) were performed using an FEI Talos transmission electron microscope operated at 200 kV. Film fragments were scraped from the substrates and loaded onto carbon-coated copper grids. Elemental distribution was investigated using an FEI Talos EDX detector through elemental mapping. TEM images and EDX data were processed using FEI Velox software (version 2.6).

2.3. Chemoresistive measurements

Gas sensing tests were conducted using a conductometric platform with interdigitated platinum (Pt) electrodes and an integrated backside heating element. The transducers were placed in a sealed test chamber connected to controlled gas supply lines.[7,8] Electrical measurements at various temperatures and gas environments were performed using an Agilent E3632A instrument. The gas response (S) was defined as the ratio R_0/R for materials exhibiting n-type behavior, where R_0 is the baseline resistance measured in dry synthetic air, and R is the resistance recorded under exposure to different gas concentrations. A comprehensive description of the transducer used for measuring the chemoresistive properties, along with details of the sensing setup and measurement protocol, is provided in the SI (Fig. S1).

3. Results and discussion

The schematic of the synthesis route for mesoporous $Nb_xTi_{1-x}O_2$ and XNiO–$Nb_xTi_{1-x}O_2$ thin films is presented in

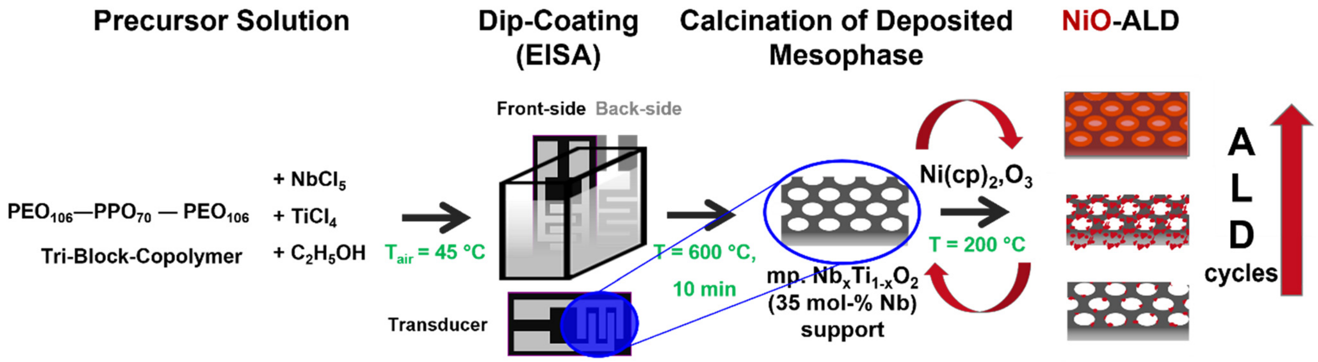

Fig. 1 Schematics of the synthesis routes for mesoporous $Nb_xTi_{1-x}O_2$ and XNiO–$Nb_xTi_{1-x}O_2$ thin films directly on the conductometric transducer.

Fig. 1. The as-synthesized mesoporous $Nb_xTi_{1-x}O_2$ exhibits a crack-free surface and a well-defined, templated mesoporous morphology with a high degree of structural homogeneity as revealed by transmission electron microscopy (TEM), Fig. 2aI and II. No collapse of the micelle-templated mesostructure occurs before oxide crystallization. The average pore diameter is 8 ± 3 nm, in line with the findings of our previous study.[14]

The mesoporous morphology of $Nb_xTi_{1-x}O_2$ remains well preserved even after the final synthesis step with NiO deposition *via* ALD, Fig. 2b and c. NiO deposition starts with the nucleation of small clusters during the initial ALD cycles (5 cycles). Due to the very small size of the deposited NiO species, identification *via* HRTEM is challenging (Fig. S2a). It is further noted that the ALD process does not essentially affect the crystallinity and mesoporosity of the $Nb_xTi_{1-x}O_2$ framework. The SAED patterns of both samples ($Nb_xTi_{1-x}O_2$ and 5NiO–$Nb_xTi_{1-x}O_2$) show similar features, with no additional diffraction rings observed after NiO deposition (Fig. S2b and c). This aligns with our earlier observations on ALD-modified mesoporous structures, for example IrTiO$_x$ modified by Ir–IrO$_x$ ALD and WC$_x$ modified by NiO ALD processes.[15,16] As the number of ALD cycles increases, these clusters grow and gradually coalesce into a continuous particulate film. This evolution is clearly observed by comparing the micrographs of the 50NiO–$Nb_xTi_{1-x}O_2$ and 200NiO–$Nb_xTi_{1-x}O_2$ samples (Fig. 2b and c). A detailed discussion of NiO ALD growth and thin film evolution can be found in our earlier work.[8,9,17]

The 50NiO–$Nb_xTi_{1-x}O_2$ sample displays discrete NiO clusters dispersed across the pore wall surface of the mesoporous $Nb_xTi_{1-x}O_2$ film (Fig. 2bI and II), while the 200NiO–$Nb_xTi_{1-x}O_2$ sample exhibits a continuous, layer-like NiO film that fully covers the mesoporous framework (Fig. 2cI and II). High-angle annular dark-field scanning transmission electron microscopy (HAADF-STEM) and the corresponding energy-dispersive X-ray spectroscopy (EDX) elemental mappings for the 50NiO–$Nb_xTi_{1-x}O_2$ sample further demonstrate conformal and homogeneous NiO

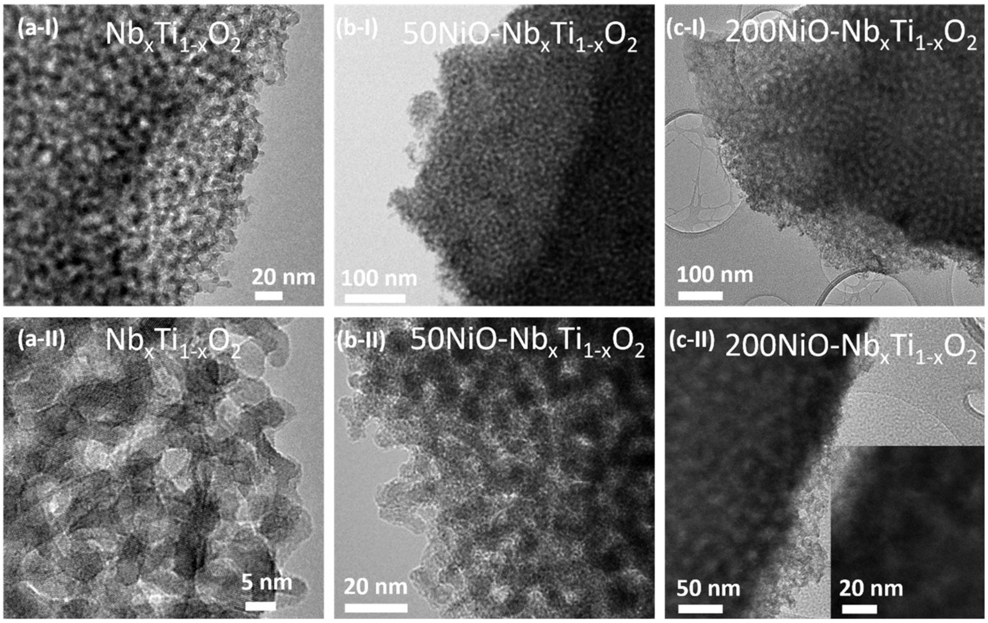

Fig. 2 BF-HRTEM images of (aI and II) $Nb_xTi_{1-x}O_2$, (bI and II) 50NiO–$Nb_xTi_{1-x}O_2$, and (cI and II) 200NiO–$Nb_xTi_{1-x}O_2$ nanostructures.

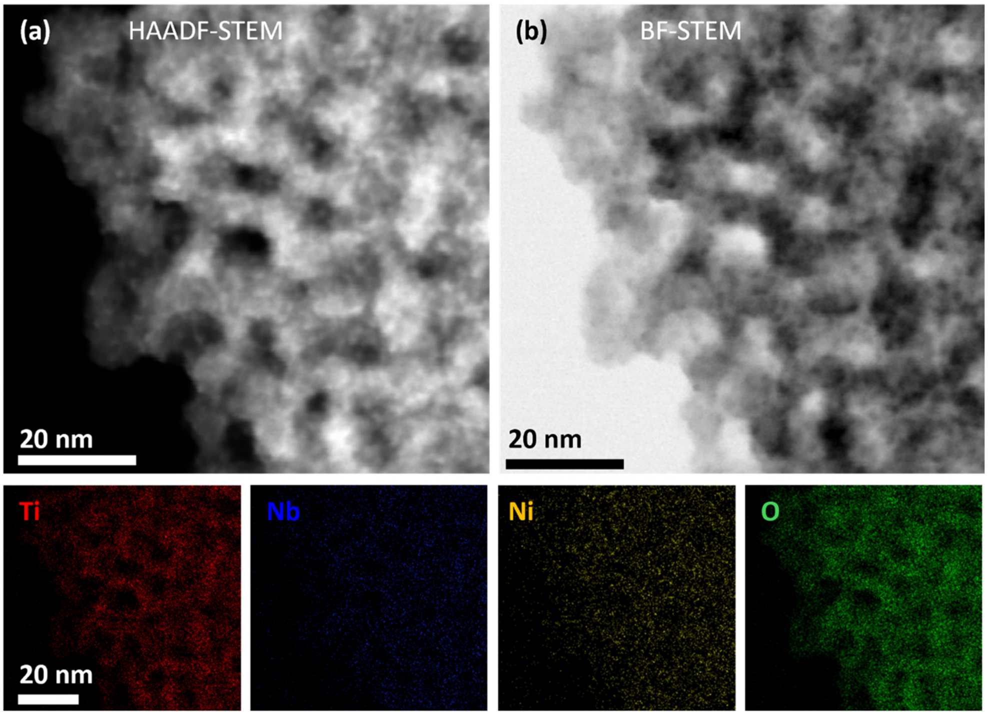

Fig. 3 (a) HAADF-STEM, (b) BF-STEM, and corresponding EDX mapping images for 50NiO–$Nb_xTi_{1-x}O_2$ thin films are shown in the bottom panel. The corresponding EDX spectra are shown in Fig. S3.

coverage across the framework (Fig. 3). The EDX mapping indicates a uniform distribution of Ni, Nb, Ti, and O within the nanostructures, consistent with the bright-field TEM micrographs shown in Fig. 2. The EDX spectra correspond to the elemental mappings in Fig. 3, and are shown in Fig. S3. Comprehensive characterization of the mesoporous $Nb_xTi_{1-x}O_2$ framework and ALD-deposited NiO, including morphology, crystallinity, and surface chemistry, is reported elsewhere.[8,9,14,17]

Fig. 4a presents the baseline resistance in dry air at various temperatures for mesoporous TiO_2, which serves as a reference having a similar pore structure and layer thickness but does not contain any Nb dopant, and for $Nb_xTi_{1-x}O_2$ as well as NiO–$Nb_xTi_{1-x}O_2$ nanostructures loaded with varying amounts of NiO. The mesoporous TiO_2 shows higher electrical resistance than Nb-doped TiO_2 ($Nb_xTi_{1-x}O_2$) in line with the computational, theoretical and practical findings on the effect of Nb doping into the TiO_2 lattice.[14] The resistance of the *X*NiO–$Nb_xTi_{1-x}O_2$ thin films with varying loadings of NiO is initially very complex particularly below 150 ALD cycles (*ca.* 3–4 nm NiO). The NiO ALD-deposition starts with NiO species nucleating initially, forming small NiO-species (5

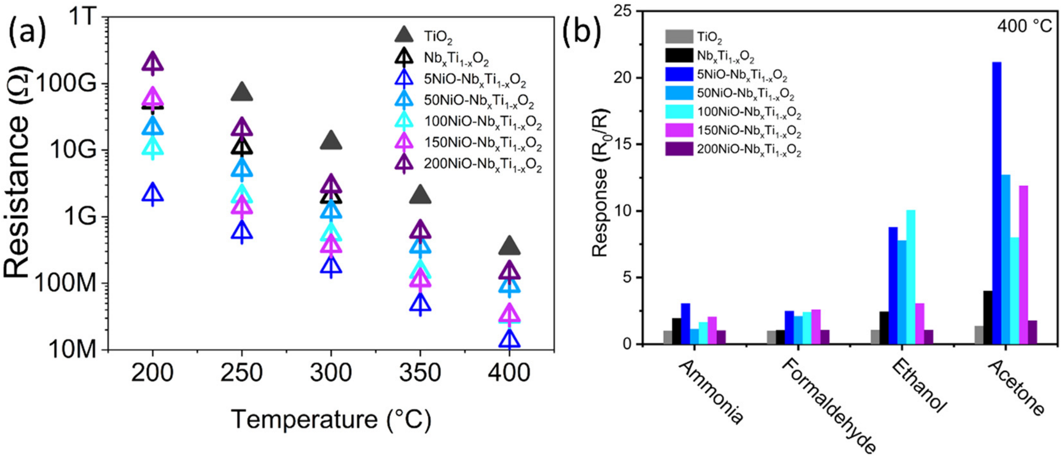

Fig. 4 (a) Electrical resistance of $Nb_xTi_{1-x}O_2$ and NiO–$Nb_xTi_{1-x}O_2$ heterostructures in dry air at a temperature range of 200–400 °C. (b) Chemoresistive sensing response of $Nb_xTi_{1-x}O_2$ and NiO–$Nb_xTi_{1-x}O_2$ nanostructures to various gases (40 ppm) including ammonia, formaldehyde, ethanol and acetone at 400 °C.

ALD cycles), which grow with additional cycles, eventually forming a particulate film (*ca.* 150 cycles).[8,15,17] Notably, partial NiO decoration of $Nb_xTi_{1-x}O_2$, where the core remains accessible, is crucial for enabling direct gas interactions with the core of the material.[2,7,18] 200NiO–$Nb_xTi_{1-x}O_2$ shows higher resistance than the unloaded $Nb_xTi_{1-x}O_2$ confirming the formation of electrical contact in between the NiO shell and the core of $Nb_xTi_{1-x}O_2$ (p–n heterojunction).[7,8,19] At this point, where the underlying sensing film is almost fully covered with the NiO coating, the diffusion of gas molecules to the core is significantly reduced (*cf.* discussion below). Our devices are designed so that electronic conduction occurs primarily through the core ($Nb_xTi_{1-x}O_2$), which directly interfaces with the metal contacts. However, NiO deposition on the mesoporous $Nb_xTi_{1-x}O_2$ creates a heterojunction, thereby increasing the overall resistance of the system by narrowing the conduction channel due to the space-charge-region at the p–n interface.[2,7]

The chemoresistive properties of $Nb_xTi_{1-x}O_2$ and NiO–$Nb_xTi_{1-x}O_2$ were studied in the presence of ammonia

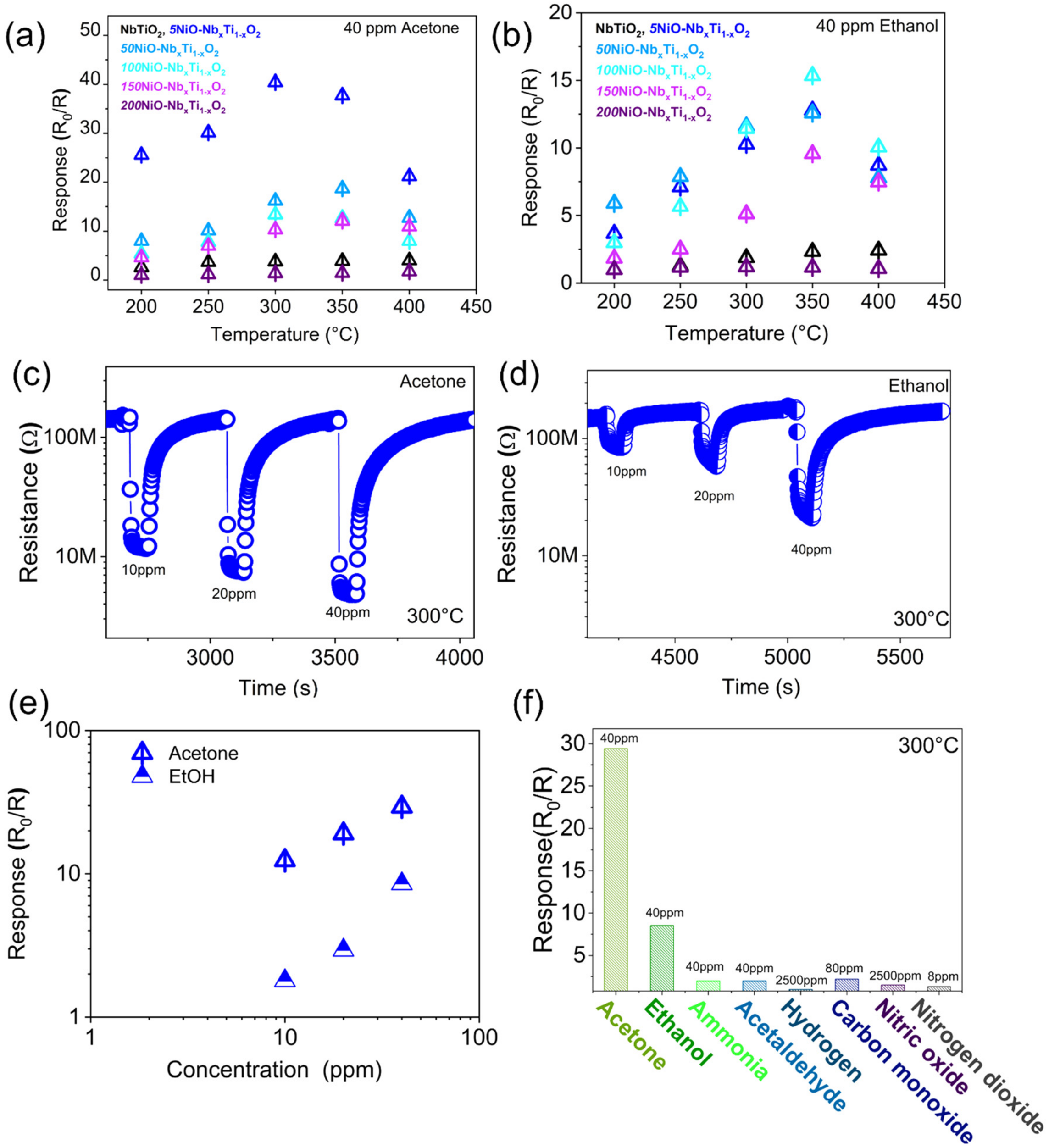

Fig. 5 Chemoresistive response of $Nb_xTi_{1-x}O_2$ and XNiO–$Nb_xTi_{1-x}O_2$ films at various temperatures in the presence of acetone (a) and ethanol (b). Isothermal dynamic response of 5NiO–$Nb_xTi_{1-x}O_2$ at 300 °C toward different concentrations of acetone (c) and ethanol (d). Calibration plots (sensing responses *vs.* acetone/ethanol concentrations) for 5NiO–$Nb_xTi_{1-x}O_2$ thin films at 300 °C (e). Response of 5NiO–$Nb_xTi_{1-x}O_2$ to acetone (40 ppm) and interfering gases, ethanol (40 ppm), ammonia (40 ppm), formaldehyde (40 ppm), hydrogen (2500 ppm), carbon monoxide (80 ppm), nitric oxide (2500 ppm) and nitrogen dioxide (8 ppm) at 300 °C, demonstrating high selectivity toward acetone (f).

(NH_3), formaldehyde (HCHO), ethanol (C_2H_5OH) and acetone (C_3H_6O), as representative reducing gases. Initial measurements were conducted at 400 °C at a concentration of 40 ppm for the above gases (Fig. 4b). Fig. 4b shows that all the samples including mesoporous $Nb_xTi_{1-x}O_2$ and NiO–$Nb_xTi_{1-x}O_2$ behave differently in the presence of various gases. The pristine mesoporous TiO_2 sensor shows the lowest response to all gases. A significant increase in response was observed upon doping the pristine TiO_2 with Nb. NiO–$Nb_xTi_{1-x}O_2$ showed a higher response toward reducing gases than non-coated $Nb_xTi_{1-x}O_2$. The response of the mesoporous NiO–$Nb_xTi_{1-x}O_2$ thin films depends on the loading of NiO, *i.e.*, the number of ALD cycles. The response of mesoporous NiO–$Nb_xTi_{1-x}O_2$ decreased with increasing ALD cycles. Notably, higher sensitivities are observed for ethanol and acetone, where the 5NiO–$Nb_xTi_{1-x}O_2$ sensor is more selective to acetone. The increased sensitivity to ethanol and acetone is attributed to the charge carriers within the nanocomposite and to the interaction of analyte with the surface species.[2,18,20,21] These results highlight the optimization of the sensing conditions to achieve selectivity toward specific gases.

The response of all the sensors toward acetone and ethanol increased up to 300–350 °C and then decreased (Fig. 5a and b). The 5NiO–$Nb_xTi_{1-x}O_2$ sensor (with 5 NiO ALD cycles) showed the highest selectivity to acetone at 300 °C (Fig. 5a and b). Therefore, all further experiments were conducted with this sensor. The isothermal dynamic response for 5NiO–$Nb_xTi_{1-x}O_2$ to different concentrations of acetone and ethanol is shown in Fig. 5c and d. Both gases exhibited similar dynamic behavior, with response/recovery times of 28 s/170 s for acetone and 33 s/175 s for ethanol, respectively. Fig. 5e presents the response *vs.* concentration curves (log–log) for acetone and ethanol, highlighting a higher sensitivity to acetone. 5NiO–$Nb_xTi_{1-x}O_2$ showed excellent selectivity for acetone at 300 °C when exposed to a mixture of gases at different concentrations (Fig. 5f). The memory effect of the 5NiO–$Nb_xTi_{1-x}O_2$ sample was studied by performing measurements at increasing and decreasing acetone concentrations, which demonstrates the sensor's signal progression over time and its stable recovery across the tested concentrations (Fig. 6a). This further confirms the repeatability of the sensor's response. Specifically, as the concentration changes from 12.5 to 400 ppm and back, the sensor exhibits consistent and repeatable responses, with practically superimposable values (Fig. 6b). The higher the concentration of acetone, the greater the response of the sensors. The calibration curves, response *versus* acetone concentration, follow a power-law relation in agreement with

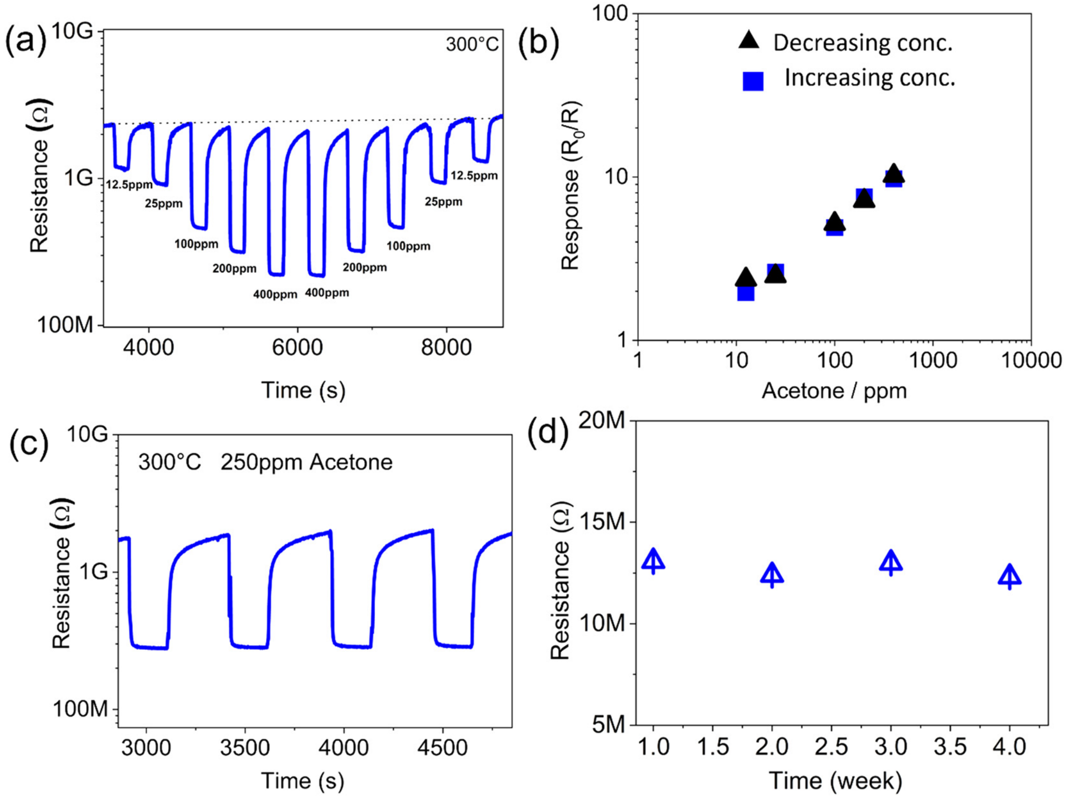

Fig. 6 (a) The memory effect of the 5NiO–$Nb_xTi_{1-x}O_2$ sensor at different increasing and decreasing concentrations of acetone, demonstrating a stable recovery across concentrations. (b) The calibration trend of the sensor's response at varying concentrations from 12.5 to 400 ppm (blue squares) and back from 400 to 12.5 ppm (black triangles); the sensor exhibits consistent and repeatable responses, with practically superimposable values. (c) Reproducibility of the sensor signals at 300 °C for 250 ppm acetone. (d) Stability of the 5NiO–$Nb_xTi_{1-x}O_2$ sensor to acetone detection, where the sensor maintains a stable response over one month, confirming long-term sensing stability.

the reported trend for SMOX-based gas sensors.[9,10] This indicates that the interaction between the gas and the sensor surface is physisorption, *i.e.*, the molecules physically adsorb onto the surface without forming strong chemical bonds.[2,6,20] Fig. 6c demonstrates the reproducibility of the sensor signals without any drift at 300 °C for 250 ppm acetone. The sensor maintained stable acetone response over one month, confirming a long-term sensing stability (Fig. 6d).

Chemoresistive sensing in SMOX occurs *via* surface reactions governed by the physicochemical properties of the SMOX surface and the nature of the analyte species. These processes range from redox reactions, such as reduction and re-oxidation of the SMOX surface (for CO and H_2), to more complex transformations involving dehydrogenation and partial oxidation (for VOCs such as ethanol and acetone). When any of these reactions involve charge transfer between SMOX and surface-adsorbed species, the concentration of charge carriers' changes, thereby modulating electrical resistance, which is the sensor signal. Details of these mechanisms, including the loaded type of heterostructures, have been reported elsewhere.[2,6,7,9,18]

TiO_2 and $Nb_xTi_{1-x}O_2$ are n-type SMOXs. In $Nb_xTi_{1-x}O_2$, resistance modulation arises from two main factors: variation in the surface depletion layer and modulation of the potential barrier across intergranular boundaries (homojunctions).[2,6] Our devices are designed such that the $Nb_xTi_{1-x}O_2$ framework remained in direct electrical contact with the electrodes, confining the dominant conduction pathway within $Nb_xTi_{1-x}O_2$, in both pristine and NiO–$Nb_xTi_{1-x}O_2$ devices. Therefore, NiO deposition modifies only the surface of the prefabricated $Nb_xTi_{1-x}O_2$ structures without directly contributing to the bulk conduction. Nevertheless, NiO can influence electrical conduction indirectly in two ways: (i) by forming a depletion layer at the p–n heterojunction, thereby modulating overall resistance,[9] and (ii) through a discontinuous (ultra-low) decoration with a secondary material, where the catalytic activity of the loaded material alters surface reactions.[2,18] In the latter case, $Nb_xTi_{1-x}O_2$ remains the primary sensing material, but resistance modulation is enhanced by the chemical or electronic sensitization of the loaded species (NiO in this case).[12,13,18]

In *X*NiO–$Nb_xTi_{1-x}O_2$ nanostructures, a p–n heterojunction is established at the NiO/$Nb_xTi_{1-x}O_2$ interface for *X* values ranging from 150 to 200, with a continuous NiO film of approximately 4–6 nm thickness (in the case of 200NiO–$Nb_xTi_{1-x}O_2$). However, this continuous NiO surface layer impedes direct analyte access to $Nb_xTi_{1-x}O_2$, thereby reducing the sensor response. Here, the primary interaction of analyte species occurs with the NiO film (p-type SMOX); however, the response remains n-type due to the predominant charge transport by $Nb_xTi_{1-x}O_2$, as dictated by the device design. At lower NiO coverages (≤100–150 ALD cycles, approximately 2–4 nm, *cf.* HRTEM in our earlier work),[8,9,17] the NiO layer is >discontinuous, comprising nanoscale NiO and $Ni(OH)_2$/NiOOH clusters (*cf.* XPS in our earlier work),[8,16,17,22] likely forming localized p–n junctions while leaving substantial areas of the $Nb_xTi_{1-x}O_2$ pore walls exposed. This configuration allows simultaneous analyte interactions with both the NiO and the mesoporous $Nb_xTi_{1-x}O_2$ film (in the case of 50NiO-$Nb_xTi_{1-x}O_2$ and 100NiO–$Nb_xTi_{1-x}O_2$).

The case of ultrathin NiO decoration (the case of 5NiO–$Nb_xTi_{1-x}O_2$ sample with 5 ALD cycles) is notably distinct. Here, the $Nb_xTi_{1-x}O_2$ surface is modified with ultra-small NiO, $Ni(OH)_2$/NiOOH and/or ionic species (Ni^{+2}/Ni^{+3}), which serve as catalytic centers.[17,22] These Ni-based species enhance oxygen ionosorption *via* spillover, thereby promoting VOC interactions at the $Nb_xTi_{1-x}O_2$ pore wall surface, resulting in the exceptionally high response observed for 5NiO–$Nb_xTi_{1-x}O_2$ (Fig. 7).[23,24] NiO/$Ni(OH)_2$ species act as oxygen dissociation catalysts, generating reactive species such as O^-, O_2^-, and O_2^{2-}, which migrate to $Nb_xTi_{1-x}O_2$ *via* spillover.[25,26] These activated species capture electrons from the conduction band of $Nb_xTi_{1-x}O_2$, and hence their reactions with target gases produce pronounced resistance changes. The enhanced sensitivity of 5NiO–$Nb_xTi_{1-x}O_2$ toward ethanol and acetone (shows a response of 40 to 40 ppm of acetone at 300 °C) thus stems from increased oxygen coverage mediated by NiO sensitization.[26–29] While acetone detection does not involve classical spillover, it still relies on spillover-activated oxygen species at the NiO/$Nb_xTi_{1-x}O_2$ interface.[26–30] For ethanol, both oxygen spillover and catalytic dehydrogenation at Ni sites contribute. Ethanol is oxidized to intermediates such as ethanal, which subsequently react with spillover oxygen to yield CO_2 and H_2 (or other by-products). This redox cycle dynamically modulates carrier density, thereby amplifying the sensor response.[23,30] Experiments, including further engineering with well-known, high-surface-area nanostructures of an active sensing material but with similar NiO loading, as well as *in situ* spectroscopic studies, will be helpful to further elucidate the underlying mechanisms. This knowledge-based design of highly efficient SMOX gas sensor

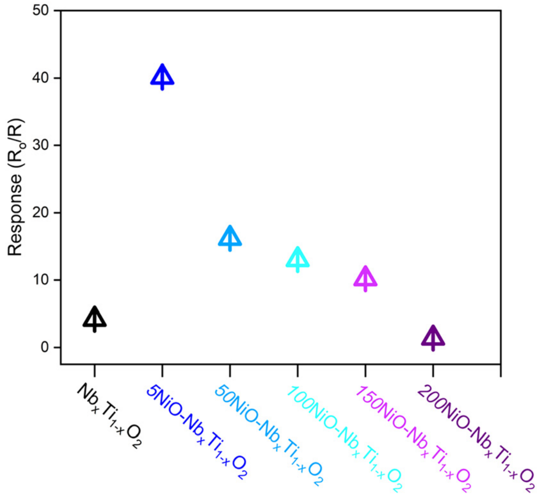

Fig. 7 Chemoresistive response of the 5NiO–$Nb_xTi_{1-x}O_2$ thin films as a function of the NiO layer thickness toward 40 ppm of acetone at 300 °C.

materials would enable the next step toward adopting thin-film technologies for practical sensing applications.

4. Conclusion

Soft-templated mesoporous Nb-doped titania ($Nb_xTi_{1-x}O_2$) thin films were fabricated on-chip on conductometric transducers and conformally loaded with NiO *via* atomic layer deposition. The on-chip fabricated NiO–$Nb_xTi_{1-x}O_2$ films showed an enhanced response to reducing gases, particularly acetone and ethanol, compared to the pristine mesoporous $Nb_xTi_{1-x}O_2$ films. Among them, 5NiO–$Nb_xTi_{1-x}O_2$, with a low NiO loading after only 5 ALD cycles, featuring discontinuous NiO-decorated species, exhibited the strongest response to acetone. The enhanced sensing performance is attributed to the incorporation of Nb dopants into the TiO_2 crystal lattice, efficient gas adsorption owing to the accessible high-surface-area mesopore structure, and chemical sensitization of the NiO species at the $Nb_xTi_{1-x}O_2$ surface in the NiO–$Nb_xTi_{1-x}O_2$ films. These findings highlight thin films as a foundation for the rational engineering of efficient SMOX gas sensors.

Conflicts of interest

There are no conflicts to declare.

Data availability

The data supporting this article have been included as part of the supplementary information (SI). Supplementary information is available. See DOI: https://doi.org/10.1039/d5lf00279f.

Acknowledgements

The authors acknowledge the financial support of the German Federal Ministry of Education and Research (BMBF) within the ATO-KAT (03EK3052A) and Catlab (03EW0015A) projects.

References

1 S. Lany, Semiconducting transition metal oxides, *J. Phys.: Condens. Matter*, 2015, **27**(28), 283203, DOI: 10.1088/0953-8984/27/28/283203.

2 D. Degler, U. Weimar and N. Barsan, Current Understanding of the Fundamental Mechanisms of Doped and Loaded Semiconducting Metal-Oxide-Based Gas Sensing Materials, *ACS Sens.*, 2019, **4**(9), 2228–2249, DOI: 10.1021/acssensors.9b00975.

3 X. Yu, T. J. Marks and A. Facchetti, Metal oxides for optoelectronic applications, *Nat. Mater.*, 2016, **15**(4), 383–396, DOI: 10.1038/nmat4599.

4 J. Zhang, X. Liu, G. Neri and N. Pinna, Nanostructured Materials for Room-Temperature Gas Sensors, *Adv. Mater.*, 2016, **28**(5), 795–831, DOI: 10.1002/adma.201503825.

5 N. Barsan, D. Koziej and U. Weimar, Metal oxide-based gas sensor research: How to?, *Sens. Actuators, B*, 2007, **121**(1), 18–35, DOI: 10.1016/j.snb.2006.09.047.

6 N. Barsan and U. Weimar, Conduction Model of Metal Oxide Gas Sensors, *J. Electroceram.*, 2001, **7**(3), 143–167, DOI: 10.1023/A:1014405811371.

7 M. H. Raza, R. Di Chio, K. Movlaee, P. Amsalem, N. Koch, N. Barsan, G. Neri and N. Pinna, Role of Heterojunctions of Core–Shell Heterostructures in Gas Sensing, *ACS Appl. Mater. Interfaces*, 2022, **14**(19), 22041–22052, DOI: 10.1021/acsami.2c00808.

8 M. H. Raza, K. Movlaee, S. G. Leonardi, N. Barsan, G. Neri and N. Pinna, Gas Sensing of NiO-SCCNT Core–Shell Heterostructures: Optimization by Radial Modulation of the Hole-Accumulation Layer, *Adv. Funct. Mater.*, 2020, **30**(6), 1906874, DOI: 10.1002/adfm.201906874, (acccessed 2025/04/18).

9 M. H. Raza, N. Kaur, E. Comini and N. Pinna, Toward Optimized Radial Modulation of the Space-Charge Region in One-Dimensional SnO2–NiO Core–Shell Nanowires for Hydrogen Sensing, *ACS Appl. Mater. Interfaces*, 2020, **12**(4), 4594–4606, DOI: 10.1021/acsami.9b19442.

10 M. H. Raza, N. Kaur, E. Comini and N. Pinna, SnO2-SiO2 1D Core-Shell Nanowires Heterostructures for Selective Hydrogen Sensing, *Adv. Mater. Interfaces*, 2021, **8**(17), 2100939, DOI: 10.1002/admi.202100939.

11 L. Mädler, A. Roessler, S. E. Pratsinis, T. Sahm, A. Gurlo, N. Barsan and U. Weimar, Direct formation of highly porous gas-sensing films by in situ thermophoretic deposition of flame-made Pt/SnO2 nanoparticles, *Sens. Actuators, B*, 2006, **114**(1), 283–295, DOI: 10.1016/j.snb.2005.05.014.

12 A. Staerz, U. Weimar and N. Barsan, Current state of knowledge on the metal oxide based gas sensing mechanism, *Sens. Actuators, B*, 2022, **358**, 131531, DOI: 10.1016/j.snb.2022.131531.

13 G. Yuan, Y. Zhong, Y. Chen, Q. Zhuo and X. Sun, Highly sensitive and fast-response ethanol sensing of porous Co3O4 hollow polyhedra via palladium reined spillover effect, *RSC Adv.*, 2022, **12**(11), 6725–6731, DOI: 10.1039/D1RA09352E.

14 M. Frisch, J. Laun, J. Marquardt, A. Arinchtein, K. Bauerfeind, D. Bernsmeier, M. Bernicke, T. Bredow and R. Kraehnert, Bridging experiment and theory: enhancing the electrical conductivities of soft-templated niobium-doped mesoporous titania films, *Phys. Chem. Chem. Phys.*, 2021, **23**(5), 3219–3224, DOI: 10.1039/D0CP06544G.

15 M. Frisch, M. H. Raza, M.-Y. Ye, R. Sachse, B. Paul, R. Gunder, N. Pinna and R. Kraehnert, ALD-Coated Mesoporous Iridium-Titanium Mixed Oxides: Maximizing Iridium Utilization for an Outstanding OER Performance, *Adv. Mater. Interfaces*, 2022, **9**(6), 2102035, DOI: 10.1002/admi.202102035, (acccessed 2025/04/18).

16 M. Frisch, M.-Y. Ye, M. H. Raza, A. Arinchtein, D. Bernsmeier, A. Gomer, T. Bredow, N. Pinna and R. Kraehnert, Mesoporous WC Films with NiO-Protected Surface: Highly Active Electrocatalysts for the Alkaline Oxygen Evolution Reaction, *ChemSusChem*, 2021, **14**(21), 4708–4717, DOI: 10.1002/cssc.202101243, (acccessed 2025/04/18).

17 M. H. Raza, K. Movlaee, Y. Wu, S. M. El-Refaei, M. Karg, S. G. Leonardi, G. Neri and N. Pinna, Tuning the NiO Thin Film Morphology on Carbon Nanotubes by Atomic Layer Deposition for Enzyme-Free Glucose Sensing, *ChemElectroChem*, 2019, **6**(2), 383–392, DOI: 10.1002/celc.201801420, (acccessed 2025/04/18).

18 D. Degler, U. Geyik, B. Junker-Reiss, M. H. Raza, P. Amsalem, N. Koch, B. Detlefs, N. Pinna, U. Weimar and N. Barsan, Investigation on the Structure–Function Relationship of Atomic-Layer-Deposited Platinum Additives on Tungsten Trioxide Gas Sensor Materials, *J. Phys. Chem. C*, 2025, **129**(34), 15301–15308, DOI: 10.1021/acs.jpcc.5c05000.

19 A. Staerz, X. Gao, F. Cetmi, Z. Ming, U. Weimar, T. Zhang and N. Barsan, Dominant Role of Heterojunctions in Gas Sensing with Composite Materials, *ACS Appl. Mater. Interfaces*, 2020, **12**(18), 21127–21132, DOI: 10.1021/acsami.0c05173.

20 T. Russ, M. Zhang, T. Zhou, U. Weimar, T. Zhang and N. Barsan, 7 - Fabrication of metal oxide heterostructures for the application in chemoresistive gas sensors. in *Metal Oxide-Based Heterostructures*, ed. N. Kumar, B. M. Soucase and G. Korotcenkov, Elsevier, 2023, pp. 247–295.

21 E. A. Schmitt, M. Krott, M. Epifani, K. Suematsu, U. Weimar and N. Barsan, Volatile Organic Compound Sensing with WO3-Based Gas Sensors: Surface Chemistry Basics, *J. Phys. Chem. C*, 2024, **128**(4), 1633–1643, DOI: 10.1021/acs.jpcc.3c06954.

22 Y. Fan, Y. Wu, G. Clavel, M. H. Raza, P. Amsalem, N. Koch and N. Pinna, Optimization of the Activity of Ni-Based Nanostructures for the Oxygen Evolution Reaction, *ACS Appl. Energy Mater.*, 2018, **1**(9), 4554–4563, DOI: 10.1021/acsaem.8b00666.

23 Q. Li, W. Zeng, Q. Zhou and Z. Wang, Highly Sensitive Ethanol Sensing Using NiO Hollow Spheres Synthesized via Hydrothermal Method, *Chem*, 2022, **10**(8), 341.

24 Q. Li, W. Zeng and Y. Li, NiO-Based Gas Sensors for Ethanol Detection: Recent Progress, *J. Sens.*, 2022, **2022**(1), 1855493, DOI: 10.1155/2022/1855493.

25 K.-D. Kim, J. W. Nam, H. O. Seo, Y. D. Kim and D. C. Lim, Oxidation of Toluene on Bare and TiO2-Covered NiO-Ni(OH)2 Nanoparticles, *J. Phys. Chem. C*, 2011, **115**(46), 22954–22959, DOI: 10.1021/jp2065997.

26 R. Qin, J. Chen, X. Gao, X. Zhu, X. Yu and K. Cen, Catalytic oxidation of acetone over CuCeOx nanofibers prepared by an electrospinning method, *RSC Adv.*, 2014, **4**(83), 43874–43881, DOI: 10.1039/C4RA04690K.

27 W. C. Conner Jr. and J. L. Falconer, Spillover in Heterogeneous Catalysis, *Chem. Rev.*, 1995, **95**(3), 759–788, DOI: 10.1021/cr00035a014.

28 P. C. M. Laan, F. J. de Zwart, E. M. Wilson, A. Troglia, O. C. M. Lugier, N. J. Geels, R. Bliem, J. N. H. Reek, B. de Bruin, G. Rothenberg and N. Yan, Understanding the Oxidative Properties of Nickel Oxyhydroxide in Alcohol Oxidation Reactions, *ACS Catal.*, 2023, **13**(13), 8467–8476, DOI: 10.1021/acscatal.3c01120.

29 G. Li, X. Wang, L. Liu, R. Liu, F. Shen, Z. Cui, W. Chen and T. Zhang, Controllable Synthesis of 3D Ni(OH)2 and NiO Nanowalls on Various Substrates for High-Performance Nanosensors, *Small*, 2015, **11**(6), 731–739, DOI: 10.1002/smll.201400830.

30 X. Mu, H. Ding, W. Pan, Q. Zhou, W. Du, K. Qiu, J. Ma and K. Zhang, Research progress in catalytic oxidation of volatile organic compound acetone, *J. Environ. Chem. Eng.*, 2021, **9**(4), 105650, DOI: 10.1016/j.jece.2021.105650.